Nuclear Engineering and Technology xxx (xxxx) xxx

Contents lists available at ScienceDirect

Nuclear Engineering and Technology

journal homepage: www.elsevier.com/locate/net

New algorithm to estimate proton beam range for multi-slit prompt-gamma camera

Youngmo Ku, Jaerin Jung, Chan Hyeong Kim*

[a] Department of Nuclear Engineering, Hanyang University, Seoul, 04763, South Korea

ARTICLE INFO

Article history:
Received 27 December 2021
Received in revised form
25 March 2022
Accepted 25 April 2022
Available online xxx

Keywords:
Proton therapy
Range uncertainty
Prompt gamma imaging
Multi-slit prompt-gamma camera
Range estimation
Monte Carlo simulation

ABSTRACT

The prompt gamma imaging (PGI) technique is considered as one of the most promising approaches to estimate the range of proton beam in the patient and unlock the full potential of proton therapy. In the PGI technique, a dedicated algorithm is required to estimate the range of the proton beam from the prompt gamma (PG) distribution acquired by a PGI system. In the present study, a new range estimation algorithm was developed for a multi-slit prompt-gamma camera, one of PGI systems, to estimate the range of proton beam with high accuracy. The performance of the developed algorithm was evaluated by Monte Carlo simulations for various beam/phantom combinations. Our results generally show that the developed algorithm is very robust, showing very high accuracy and precision for all the cases considered in the present study. The range estimation accuracy of the developed algorithm was 0.5−1.7 mm, which is approximately 1% of beam range, for 1×10^9 protons. Even for the typical number of protons for a spot (1×10^8), the range estimation accuracy of the developed algorithm was 2.1−4.6 mm and smaller than the range uncertainties and typical safety margin, while that of the existing algorithm was 2.5−9.6 mm.

1. Introduction

The existence of Bragg peak followed by a steep falloff of depth-dose distribution makes protons favorable for cancer therapy. On the other hand, it also makes the proton therapy susceptible to errors in beam range (i.e., penetration depth in the patient). The errors that arise from imperfect conversion of CT numbers to stopping power, inaccurate patient positioning, and inter-fractional anatomical changes, etc. force prescription of relatively high dose to healthy tissues near the treatment target volume in order to ensure the robustness of treatment in clinical practice [1]. Therefore, the reduction of range uncertainties can be translated into a more conformal dose delivery to the target volume and a better treatment outcome. Recently, quantitative benefits from the reduction of range uncertainties have been reported in terms of healthy tissue dose and normal tissue complication probability (NTCP) [2].

To reduce range uncertainties, the *in vivo* range verification technique based on imaging of prompt gamma rays (PGs) has been investigated by many research groups [3] since it was first proposed by Stichelbaut and Jongen [4] and experimentally demonstrated by Min et al. [5]. Until now, the prompt gamma imaging (PGI) has been acknowledged as one of the most promising approaches for range verification because the distribution of PG emission is highly correlated with depth dose distribution. Additionally, the method is capable of real-time monitoring of beam range because the PGs are emitted within a few nanoseconds after proton-tissue interaction. Our previous study [6] developed a PGI system, called a multi-slit prompt-gamma camera, which estimates the range of proton beam by measuring the depth distribution of PGs using a parallel-slit collimator and multiple scintillation detectors and demonstrated its capability for measuring the range of therapeutic proton beam. The development of PGI systems such as a knife-edge camera [7,8], a Compton camera [9], a gamma electron vertex imaging (GEVI) system [10,11], and others [3,12] also have been reported.

The PGI systems require a dedicated algorithm to estimate the range of proton beam from the measured PG distribution. In the knife-edge camera, a shifting algorithm is used to estimate the range of the proton beam in a patient, which estimates the range of the proton beam by shifting the measured PG distribution toward the reference PG distribution which is produced by Monte Carlo simulation. The accuracy of this approach is, however, limited by the accuracy of Monte Carlo simulation which is prone to errors when a very complicated geometry, like a human head, is involved. Meanwhile, the multi-slit prompt-gamma camera uses a fitting algorithm, which estimates the range by fitting the PG distribution

* Corresponding author.
E-mail address: chkim@hanyang.ac.kr (C.H. Kim).

https://doi.org/10.1016/j.net.2022.04.019

in the distal falloff region using a sigmoidal curve [13]. The advantage of this algorithm is that it estimates the beam range without referring to a reference PG distribution. Despite this advantage, however, the fitting algorithm is not sufficiently stable, resulting in the failure of curve-fitting in harsh circumstances, i.e., insufficient counting statistics. For the typical number of protons (1×10^8) in a spot in spot scanning proton therapy, for example, the accuracy of the fitting algorithm was not enough to reduce range uncertainties in the clinic [6].

In the present study, a new range estimation algorithm was developed for the multi-slit prompt-gamma camera, which overcomes the limitation of the existing algorithm and estimates the range of proton beam with higher precision. The developed algorithm is based on a very simple recipe involving derivation, smoothing, and centroid calculation. The performance of the developed algorithm was evaluated by Monte Carlo simulations for various beam/phantom combinations. The accuracy of the developed algorithm was also compared with that of the fitting algorithm and also with range uncertainties and typical safety margin [1] in proton therapy.

2. Materials and methods

2.1. Range definition

The range of a proton beam is defined at the position where the dose has decreased to 80% of the maximum dose, i.e. in the distal dose falloff, which coincides with the mean projected range of a proton for a monoenergetic proton beam [1]. Range uncertainty is the amount of unpredictability for range in the clinic, and 2.4% of beam range +1.2 mm (1.5 standard deviations) that was evaluated by Paganetti et al. [1] was adopted in the present study. In this paper, the true range is the range of a proton beam calculated by the above definition from a depth-dose distribution that was acquired in a simulation. The planned range is the range of a proton beam predicted in the treatment planning stage, and it intrinsically has uncertainty in the clinic. To consider this uncertainty, in this paper, the planned range was set to a true range added by a value generated by Gaussian random sampling with a standard deviation of range uncertainty. The estimated range is the value of a range estimated by the multi-slit prompt gamma camera using the developed algorithm.

2.2. Range estimation algorithm

To estimate the range of proton beam from a PG distribution acquired by a multi-slit prompt-gamma camera, the present study proposes a new algorithm, which is composed of three steps described below:

i. The first derivative of the PG distribution is produced using the centered finite difference approximation. The profile is then smoothed with a Gaussian filter ($\sigma = 5$ mm) to reduce statistical fluctuation (see Fig. 1). The width of the filter was

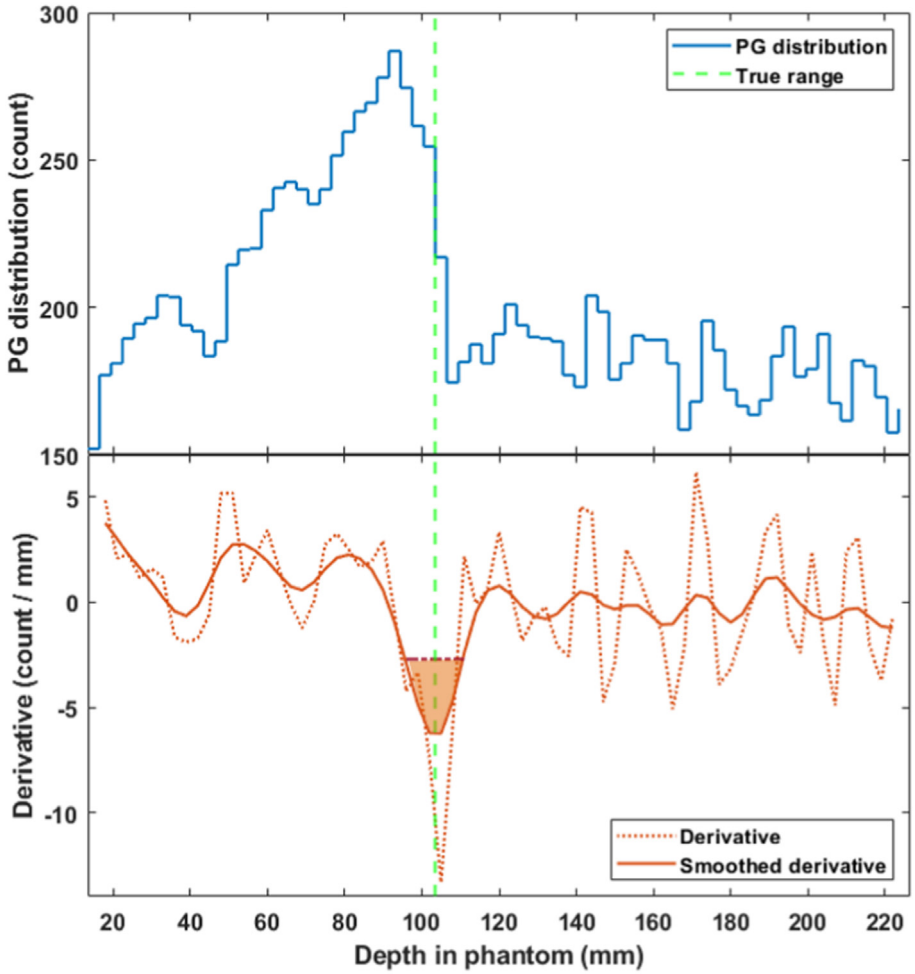

Fig. 1. Principle of developed algorithm to estimate proton beam range. PG distribution and its derivative are displayed in upper and lower half, respectively.

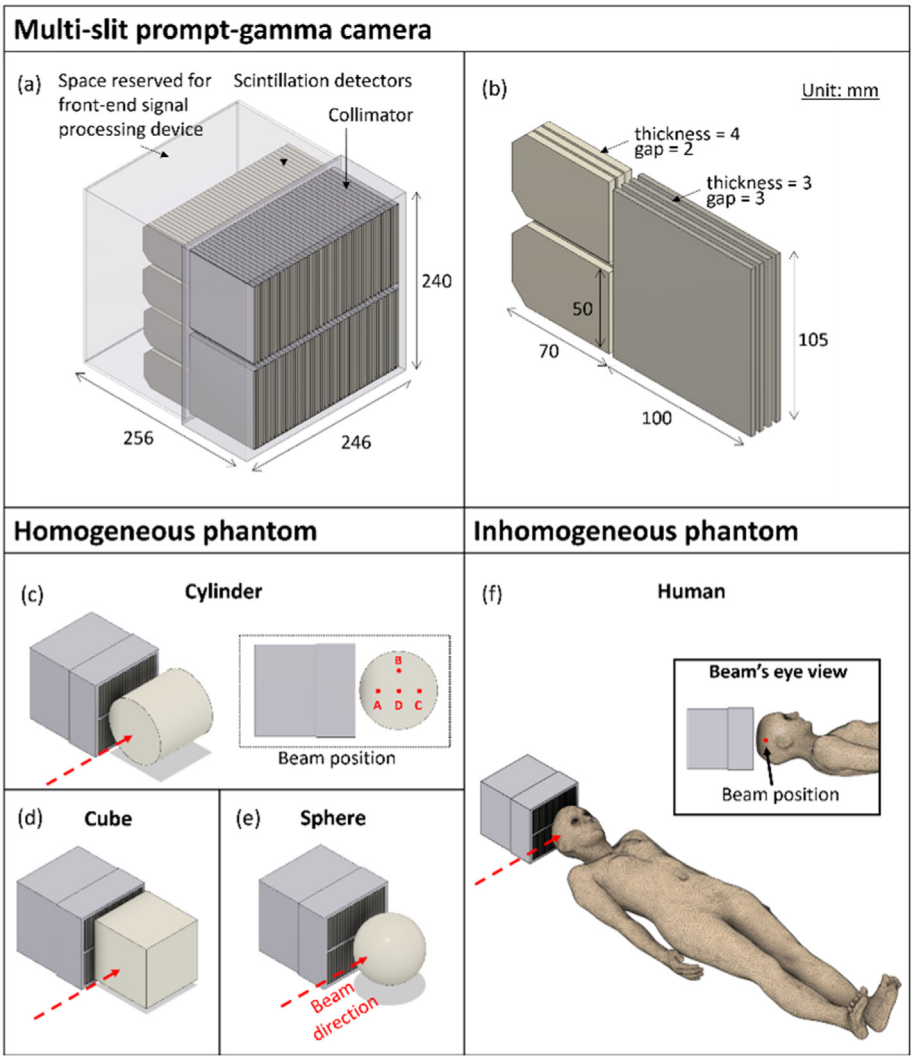

Fig. 2. Geometry of multi-slit prompt-gamma camera in simulation (a) and configuration of tungsten plates (components of collimator) and scintillation detectors (b). Geometrical setup of multi-slit prompt gamma camera to measure proton beam range in cylindrical phantom (c), cubic phantom (d), spherical phantom (e), and mesh-type reference computational phantom (f).

determined at smaller than the spatial resolution of the camera in PG measurement (8.5 mm) to avoid significant loss of spatial information by the filter. A similar example can be found in the reference [14].

ii. The deepest valley is selected within the region which covers the 99.99% confidence interval (4σ) of the planned range in the patient. If there is no valley in that region, the deepest valley in the entire profile is selected. Note that the extent of the region can be adjusted at each hospital according to the range uncertainties evaluated in the hospital. In the present study, the extent was determined based on the range uncertainties documented by Paganetti et al. [1].

iii. The range of the proton beam is estimated as the centroid of the lower half of the selected valley (i.e., shaded area in Fig. 1).

To compare range estimation accuracy, the existing fitting algorithm was also employed to estimate range from PG distribution [6,13]. Note that the existing algorithm that used in this paper was identical to that used in the references including its source code.

2.3. Evaluation of algorithm using Monte Carlo simulation

The developed algorithm was evaluated under various conditions by simulating the PG measurement of the multi-slit prompt-gamma camera (Fig. 2a and b) with the Geant4 Monte Carlo simulation toolkit (ver. 10.05.p02) [15]. The accuracy of the algorithm was evaluated using a homogeneous cylindrical phantom for different beam energies, the numbers of protons, and beam positions (Fig. 2c). The algorithm was also evaluated using three different shapes of phantoms (cylinder, cubic, and sphere; Fig. 2c–e) to examine its dependency on the shape of the object. In addition, the applicability of the algorithm to a close-to-clinic condition was investigated using a mesh-type reference computational phantom (Fig. 2f) [16]. Finally, the accuracy of the developed algorithm was compared with that of the existing sigmoidal curve-fitting algorithm and also with range uncertainties and typical safety margins [1] in proton therapy. Further details are provided in the following.

Fig. 2a and b shows the geometry of the multi-slit prompt-

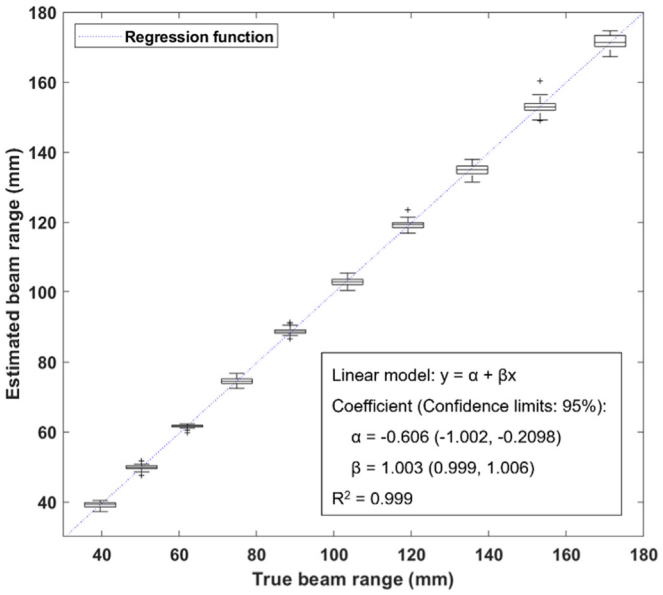

Fig. 3. Box plot of estimated beam ranges for different proton beam energies (i.e., different true beam ranges). Object was cylindrical phantom. Result of linear regression is also displayed.

gamma camera in simulation. The camera consists of a multi-slit collimator and an array of scintillation detectors. The collimator comprises 72 tungsten plates ($3 \times 100 \times 105$ mm^3, $\rho = 19.25$ g/cm^3) to construct two rows of parallel slits (2×36) in a staggered layout, providing a 3 mm data pitch. Two CsI(Tl) scintillation detectors are placed behind each slit to detect PGs passing through the slit. The scintillators have a wedge-shaped end in consideration of the active area of photodiodes (S3588-08, Hamamatsu, Japan, active area $= 3 \times 30$ mm^2). The camera measures the PG distribution by counting the number of events in which the energy deposited in the detector is within the range of 3–10 MeV.

Fig. 2c–f shows the geometrical setup of the camera, beam positions, and phantoms: (c) cylindrical phantom (d, h = 20 cm), (d) cubic phantom (l = 20 cm), (e) spherical phantom (d = 20 cm), and (f) a mesh-type reference computational phantom (adult female) [16]. The simple solid phantoms (c–e) were homogeneous phantoms filled with average soft tissue (adult female, ICRU-44 [17]). For homogeneous phantoms, the proton beam was pointed toward the center of the phantom, except for the positions of A, B, and C in the cylindrical phantom, which were located 5 cm away from the center. For the human phantom (f), the beam was pointed toward a point, which is 6 cm inferior from the bregma. The camera was separated from the phantom by 1 cm. The direction of the proton beam was parallel to the front face of the camera and therefore perpendicular to the collimation slits.

To calculate the true range of proton beam in a phantom, the depth-dose distribution was acquired with 0.1 mm pitch using parallel world geometry in the Geant4 simulations. The true range was determined at the location where the dose has decreased to 80% of the maximum dose in the distribution.

The reference physics list 'QGSP_BIC_HP', which is recommended for medical applications, was adopted in the simulations, as it describes well the production of secondary particles in the interactions between protons and nuclei [18,19]. The emission yield of PG was scaled down in the simulations, as they are known to be overestimated with this physics list [20]. The default settings of Geant4 were used, and variance reduction techniques were not used.

3. Results and discussion

3.1. Range estimation for different proton beam energies

The range estimation algorithm developed in the present study was examined for different proton beam energies using the cylindrical phantom with beam position D (i.e., center of the phantom). The considered beam energies ranged from 70 to 160 MeV at 10 MeV intervals, which correspond to the true ranges of 39.6, 50.3, 62.1, 74.9, 88.7, 103.5, 119.1, 135.7, 153.2, and 171.3 mm, respectively. The number of incident protons was 3×10^8 in simulation, and

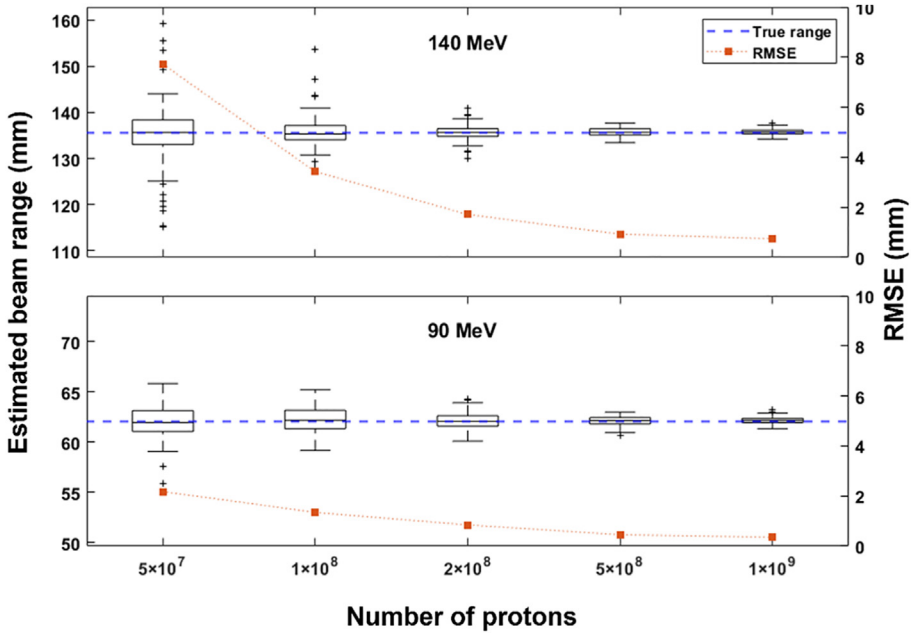

Fig. 4. Estimated beam ranges for different number of protons (5×10^7, 1×10^8, 2×10^8, 5×10^8, and 1×10^9). Object was cylindrical phantom. RMSE is displayed as well.

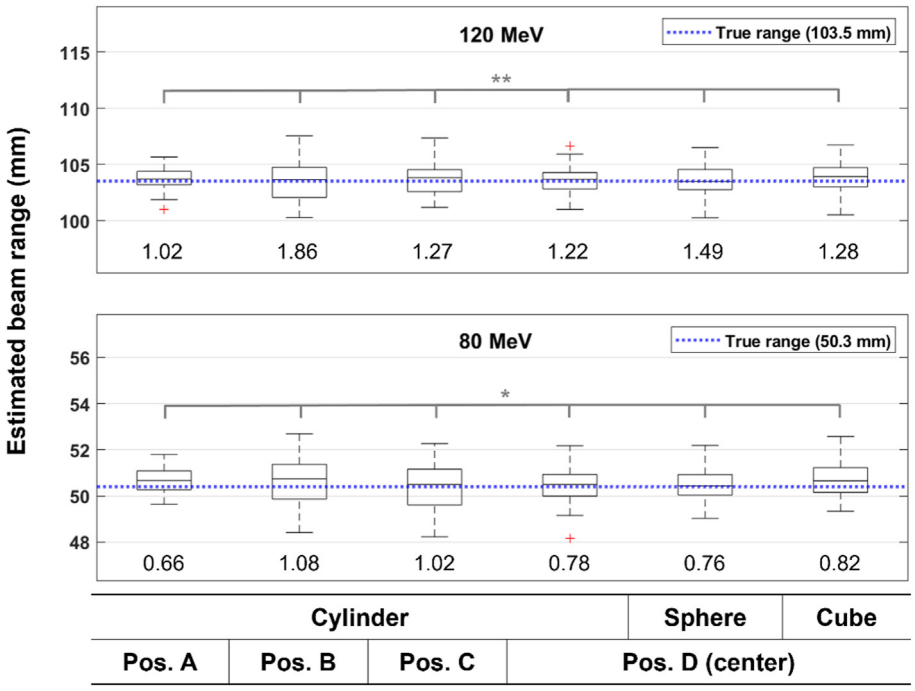

Fig. 5. Estimated beam ranges for different geometric conditions (i.e., different phantom shapes and beam positions). RMSE is also displayed below each box. Groups of results for statistical analysis are marked with * and **.

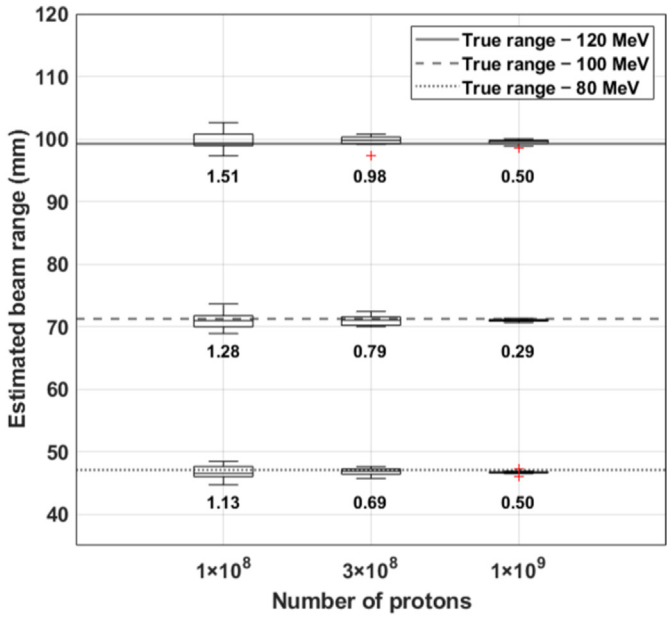

Fig. 6. Estimated beam ranges for mesh-type reference computational human phantom.

simulation was repeated 30 times for each case.

Fig. 3 shows the simulation results of the estimated beam ranges for different proton beam energies (i.e., different true beam ranges) considered in the present study. High accuracy of range estimation was observed; that is, the mean bias error (MBE) was less than 0.9 mm for all energies considered in the present study. A linear regression analysis (model function: $y = \alpha + \beta x$) indicated very high linearity of the estimated ranges with the true beam ranges over the entire energy range, showing that the slope ($\beta = 1.003$ [0.999, 1.006], confidence limits: 95%) was not statistically different from unity, and the coefficient of determination (R^2) was very high ($= 0.999$). A systemic error of -0.6 mm was observed at the y-intercept (α) in the regression and, therefore, it was corrected by adding an offset (0.6 mm) to the estimated ranges for all of the results given below. Note that it was not corrected in Fig. 3.

3.2. Range estimation for the different numbers of protons

The range estimation algorithm was examined changing the number of protons. For this, 5×10^7, 1×10^8, 2×10^8, 5×10^8, to 1×10^9 protons were irradiated to the center (i.e., position D) of the cylindrical phantom for two proton energies (90 and 140 MeV). Simulation was repeated 100 times for each case. Fig. 4 shows the simulation results of the estimated ranges in the form of a box plot and root mean square errors (RMSEs). Note that the RMSE represents the deviation of the estimated ranges from the true range and is almost identical with the standard deviation of estimation since the systematic error was removed by adding the offset. It was observed that as expected, the RMSE decreases with increasing the number of protons. For 1×10^8 protons, the RMSE was within the range of 1.3–3.4 mm. For 1×10^9 protons, which is obtainable with some statistical technique such as spot merging or aggregating [21,22], the RMSE was observed in sub-millimetric order (0.4–0.7 mm).

3.3. Range estimation for different phantom shapes and beam positions

The range estimation algorithm was evaluated for different shapes of phantoms (i.e., cylinder, cubic, and sphere, Fig. 2c–e), for which the proton beam was irradiated at the center of the phantoms. The algorithm was also evaluated for different beam positions, for which the proton beam was additionally irradiated to the A, B, and C points of the cylindrical phantom. The considered beam energies were 80 and 120 MeV (range = 50.3 and 103.5 mm), and the number of protons was 3×10^8. Simulation was repeated 30

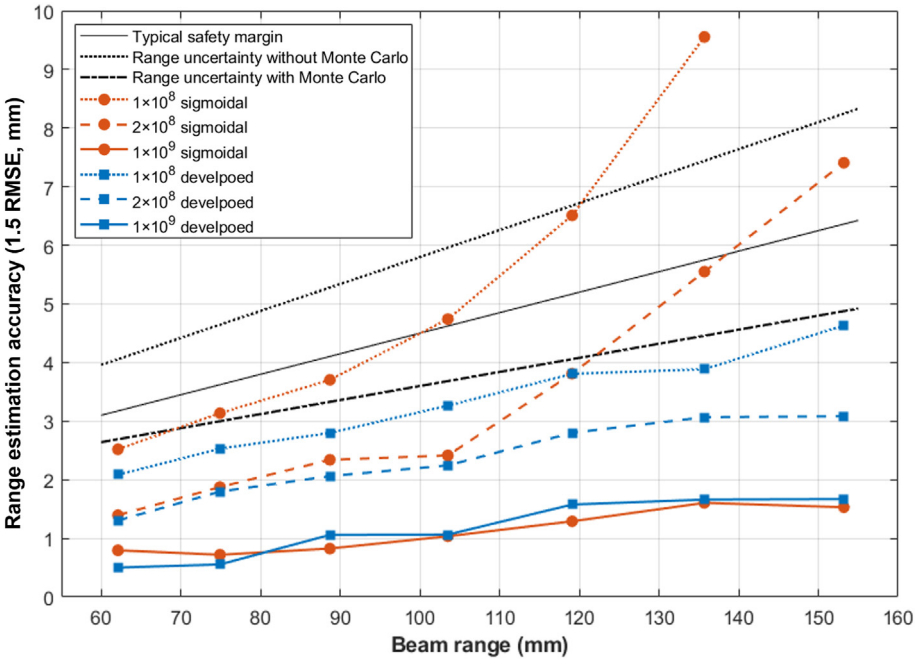

Fig. 7. Range estimation accuracy of developed algorithm in comparison with that of (sigmoidal curve) fitting algorithm. Typical safety margin for proton beam range (3.5% + 1 mm) and range uncertainty without/with Monte Carlo (4.6% + 1.2 mm, 2.4% + 1.2 mm) are also shown for comparison.

times for each case.

Fig. 5 shows the simulation results of the estimated beam ranges for the phantoms and beam positions considered in the present study, as well as RMSEs (displayed below each box). The results generally show that the range estimation is more affected by the beam position than the shape of the phantom. In addition, for the different beam positions, the RMSE of the estimated ranges was larger when the beam position was far from the camera (pos. A < D < C) or deviated from the center of the camera's field of view (pos. B), as the beam position affects the counting efficiency.

The consistency of range estimation over the geometrical conditions was examined by analyzing the differences among the mean values with statistical hypothesis tests and analysis of variance (ANOVA). ANOVA was conducted for two groups of range estimation results of the same beam energy (80 and 120 MeV) as marked above box plots (*, **) in Fig. 5. The differences between the means were not observed both in 80 ($F = 0.412$, significance probability (p) = 0.838, significance level (α) = 0.05) and 120 ($F = 0.373$, $p = 0.865$, $\alpha = 0.05$) MeV groups.

3.4. Range estimation for a human phantom

To see the applicability of the algorithm to a close-to-clinic condition, the proton beams were irradiated to the head of a mesh-type reference computational phantom. The beam position was located 6 cm inferior to the bregma of the phantom and 7 cm away from the camera. The energy of the proton beam and the number of protons were 80, 100, and 120 MeV and 1×10^8, 3×10^8, and 1×10^9, respectively. Simulation was repeated 30 times for each case.

Fig. 6 shows the beam ranges in the human phantom estimated by the developed algorithm, as well as the true ranges. As in the cases with the homogeneous phantoms, a smaller error was observed for a larger number of protons. The RMSE errors were 1.1–1.5, 0.7–1.0, and 0.3–0.5 mm for 1×10^8, 3×10^8, and 1×10^9 protons, respectively, which were comparable to those of the homogeneous phantoms. The mean bias error (MBE) was less than 0.46 mm for all cases considered in the present study.

3.5. Comparison with existing fitting algorithm, range uncertainties [1] etc.

The range estimation accuracy of the developed algorithm was compared with that of the existing fitting algorithm, as well as range uncertainties [1] and typical safety margins in proton therapy. Both algorithms were applied to the identical PG distributions which were obtained by simulating the multi-slit prompt gamma camera assuming that the cylindrical phantom was irradiated by proton beams of 80–140 MeV energy and 1×10^8, 2×10^8, and 1×10^9 protons.

Fig. 7 shows the range estimation accuracies of the developed algorithm (squares) and existing fitting algorithm (circles), as well as the range uncertainties without/with Monte Carlo simulation (4.6% + 1.2 mm, 2.4% + 1.2 mm) [1] and typical safety margins (3.5% + 1 mm) for comparison. The accuracy is plotted as 1.5 times of the RMSE for comparison with the range uncertainties and typical safety margins which are generally given as 1.5 standard deviations (94% confidence level).

For a large number of protons (1×10^9), the range estimation accuracies of the existing and developed algorithms ranged from 0.7 to 1.7 and 0.5–1.7 mm, which were comparable. The accuracies deteriorated as beam range increased, but the ratio of the accuracy to the beam range was maintained at approximately 1%. When the number of protons decreased down to 2×10^8, however, the developed algorithm showed much better accuracy (1.3–3.1 mm) than the fitting algorithm (1.4–7.4 mm), which was more evident at deeper beam ranges, i.e., higher beam energies. Note that the background signals are more prominent for higher proton energy and contribute to the low precision of the fitting algorithm by blurring the falloff edge in the PG distribution. Even for the typical number of protons for a spot (1×10^8), the range estimation accuracy of the developed algorithm (2.1–4.6 mm) was smaller than the range uncertainties [1] and typical safety margin. On the other hand, the accuracy of the existing algorithm was 2.5–9.6 mm, and it was larger than the range uncertainties and typical safety margin in most cases.

4. Conclusion

In the present study, a new range estimation algorithm for a multi-slit prompt-gamma camera was developed to estimate the range of therapeutic proton beams. The performance of the developed algorithm was evaluated for various beam/phantom combinations using the Geant4 Monte Carlo simulation toolkit. Our results generally show that the developed algorithm is very robust showing very high accuracy and precision for all the cases considered in the present study. The range estimation accuracy of the developed algorithm was 0.5–1.7 mm, which is approximately 1% of beam range, for 1×10^9 protons. Even for the typical number of protons for a spot (1×10^8), the range estimation accuracy of the developed algorithm was 2.1–4.6 mm and smaller than the range uncertainties and typical safety margin, while that of the existing curve fitting algorithm was 2.5–9.6 mm. Future work will include experimental validation with therapeutic proton beams under clinical conditions.

Declaration of competing interest

The authors declare that they have no known competing financial interests or personal relationships that could have appeared to influence the work reported in this paper.

Acknowledgments

This research was supported by Field-oriented Technology Development Project for Customs Administration through National Research Foundation of Korea (NRF) funded by the Ministry of Science & ICT and Korea Customs Service (NRF-2021M3I1A1097895), and additionally, by the National Research Foundation of Korea (NRF) grant funded by the Korea government (MSIT) (NRF-2019M2D2A1A02059814). This research was additionally supported by the National Cancer Center Grants (NCC-2110390-2), Korea.

References

[1] H. Paganetti, Range uncertainties in proton therapy and the role of Monte Carlo simulations, Phys. Med. Biol. 57 (2012), https://doi.org/10.1088/0031-9155/57/11/R99.
[2] S. Tattenberg, T.M. Madden, B.L. Gorissen, T. Bortfeld, K. Parodi, J. Verburg, Proton range uncertainty reduction benefits for skull base tumors in terms of normal tissue complication probability (NTCP) and healthy tissue doses, Med. Phys. (2021), https://doi.org/10.1002/mp.15097.
[3] J. Krimmer, D. Dauvergne, J.M. Létang, Testa, Prompt-gamma monitoring in hadrontherapy: a review, Nucl. Instr. Meth. Phys. Res. Sect. A Accel. Spectrometers, Detect. Assoc. Equip. 878 (2018) 58–73, https://doi.org/10.1016/j.nima.2017.07.063.
[4] F. Stichelbaut, Y. Jongen, Verification of the proton beam position in the patient by the detection of prompt gamma rays emission, in: 39th Meet. Part. Ther. Co-op. Gr. (San Fr, 2003, pp. 1–5.
[5] C.H. Min, C.H. Kim, M.Y. Youn, J.W. Kim, Prompt gamma measurements for locating the dose falloff region in the proton therapy, Appl. Phys. Lett. 89 (2006) 2–5, https://doi.org/10.1063/1.2378561.
[6] J.H. Park, S.H. Kim, Y. Ku, C.H. Kim, H.R. Lee, J.H. Jeong, S.B. Lee, D.H. Shin, Multi-slit prompt-gamma camera for locating of distal dose falloff in proton therapy, Nucl. Eng. Technol. 51 (2019) 1406–1416, https://doi.org/10.1016/j.net.2019.03.008.
[7] I. Perali, A. Celani, P. Busca, C. Fiorini, A. Marone, M. Basilavecchia, T. Frizzi, F. Roellinghoff, J. Smeets, D. Prieels, F. Stichelbaut, F. Vander Stappen, S. Henrotin, A. Benilov, Prompt gamma imaging with a slit camera for real-time range control in proton therapy: experimental validation up to 230 MeV with HICAM and development of a new prototype, IEEE Nucl. Sci. Symp. Conf. Rec. (2012) 3883–3886, https://doi.org/10.1109/NSSMIC.2012.6551890.
[8] Y. Xie, E.H. Bentefour, G. Janssens, J. Smeets, F. Vander Stappen, L. Hotoiu, L. Yin, D. Dolney, S. Avery, F. O'Grady, D. Prieels, J. McDonough, T.D. Solberg, R.A. Lustig, A. Lin, B.K.K. Teo, Prompt gamma imaging for in vivo range verification of pencil beam scanning proton therapy, Int. J. Radiat. Oncol. Biol. Phys. 99 (2017) 210–218, https://doi.org/10.1016/j.ijrobp.2017.04.027.
[9] P. Maggi, S. Peterson, R. Panthi, D. Mackin, H. Yang, Z. He, S. Beddar, J. Polf, Computational model for detector timing effects in Compton-camera based prompt-gamma imaging for proton radiotherapy, Phys. Med. Biol. 65 (2020), https://doi.org/10.1088/1361-6560/ab8bf0.
[10] C.H. Kim, H.R. Lee, S.H. Kim, J.H. Park, S. Cho, W.G. Jung, Gamma electron vertex imaging for in-vivo beam-range measurement in proton therapy: experimental results, Appl, Phys. Lett. 113 (2018), https://doi.org/10.1063/1.5039448.
[11] S.H. Kim, J.H. Jeong, Y. Ku, J. Jung, S. Cho, K. Jo, C.H. Kim, Upgrade of gamma electron vertex imaging system for high-performance range verification in pencil beam scanning proton therapy, Nucl. Eng. Technol. (2021), https://doi.org/10.1016/j.net.2021.09.001.
[12] A.C. Knopf, A. Lomax, In vivo proton range verification: a review, Phys. Med. Biol. 58 (2013) 131–160, https://doi.org/10.1088/0031-9155/58/15/R131.
[13] C.H. Min, H.R. Lee, C.H. Kim, S.B. Lee, Development of array-type prompt gamma measurement system for in vivo range verification in proton therapy, Med. Phys. 39 (2012) 2100–2107, https://doi.org/10.1118/1.3694098.
[14] I. Perali, A. Celani, L. Bombelli, C. Fiorini, F. Camera, E. Clementel, S. Henrotin, G. Janssens, D. Prieels, F. Roellinghoff, J. Smeets, F. Stichelbaut, F. Vander Stappen, Prompt gamma imaging of proton pencil beams at clinical dose rate, Phys. Med. Biol. 59 (2014) 5849–5871, https://doi.org/10.1088/0031-9155/59/19/5849.
[15] S. Agostinelli, J. Allison, K. Amako, J. Apostolakis, H. Araujo, P. Arce, M. Asai, D. Axen, S. Banerjee, G. Barrand, F. Behner, L. Bellagamba, J. Boudreau, L. Broglia, A. Brunengo, H. Burkhardt, S. Chauvie, J. Chuma, R. Chytracek, G. Cooperman, G. Cosmo, P. Degtyarenko, A. Dell'Acqua, G. Depaola, D. Dietrich, R. Enami, A. Feliciello, C. Ferguson, H. Fesefeldt, G. Folger, F. Foppiano, A. Forti, S. Garelli, S. Giani, R. Giannitrapani, D. Gibin, J.J. Gomez Cadenas, I. Gonzalez, G. Gracia Abril, G. Greeniaus, W. Greiner, V. Grichine, A. Grossheim, S. Guatelli, P. Gumplinger, R. Hamatsu, K. Hashimoto, H. Hasui, A. Heikkinen, A. Howard, V. Ivanchenko, A. Johnson, F.W. Jones, J. Kallenbach, N. Kanaya, M. Kawabata, Y. Kawabata, M. Kawaguti, S. Kelner, P. Kent, A. Kimura, T. Kodama, R. Kokoulin, M. Kossov, H. Kurashige, E. Lamanna, T. Lampen, V. Lara, V. Lefebure, F. Lei, M. Liendl, W. Lockman, F. Longo, S. Magni, M. Maire, E. Medernach, K. Minamimoto, P. Mora de Freitas, Y. Morita, K. Murakami, M. Nagamatu, R. Nartallo, P. Nieminen, T. Nishimura, K. Ohtsubo, M. Okamura, S. O'Neale, Y. Oohata, K. Paech, J. Perl, A. Pfeiffer, M.G. Pia, F. Ranjard, A. Rybin, S. Sadilov, E. di Salvo, G. Santin, T. Sasaki, N. Savvas, Y. Sawada, S. Scherer, S. Sei, V. Sirotenko, D. Smith, N. Starkov, H. Stoecker, J. Sulkimo, M. Takahata, S. Tanaka, E. Tcherniaev, E. Safai Tehrani, M. Tropeano, P. Truscott, H. Uno, L. Urban, P. Urban, M. Verderi, A. Walkden, W. Wander, H. Weber, J.P. Wellisch, T. Wenaus, D.C. Williams, D. Wright, T. Yamada, H. Yoshida, D. Zschiesche, GEANT4 - a simulation toolkit, Nucl. Instr. Meth. Phys. Res. Sect. A Accel. Spectrometers, Detect. Assoc. Equip. 506 (2003) 250–303, https://doi.org/10.1016/S0168-9002(03)01368-8.
[16] C.H. Kim, Y.S. Yeom, N. Petoussi-Henss, M. Zankl, W.E. Bolch, C. Lee, C. Choi, T.T. Nguyen, K. Eckerman, H.S. Kim, M.C. Han, R. Qiu, B.S. Chung, H. Han, B. Shin, ICRP publication 145: adult mesh-type reference computational phantoms, Ann. ICRP 49 (2020) 13–201, https://doi.org/10.1177/0146645319893605.
[17] D.R. White, J. Booz, R. V Griffith, J.J. Spokas, I.J. Wilson, ICRU Report 44: tissue substitutes in radiation dosimetry and measurement, J. Int. Comm. Radiat. Units Meas. 23 (1989).
[18] Cern, Geant4 Reference Physics Lists, 2013.
[19] G. collaboration, Physics Lists - Use Cases - Reference Physics Lists, ((n.d.)).
[20] M. Pinto, D. Dauvergne, N. Freud, J. Krimmer, J.M. Létang, E. Testa, Assessment of Geant4 prompt-gamma emission yields in the context of proton therapy monitoring, Front. Oncol. 6 (2016) 1–7, https://doi.org/10.3389/fonc.2016.00010.
[21] S.H. Kim, J.H. Park, Y. Ku, H.S. Lee, Y. Kim, C.H. Kim, J.H. Jeong, Improvement of statistics in proton beam range measurement by merging prompt gamma distributions: a preliminary study, J. Radiat. Prot. Res. 44 (2019) 1–7, https://doi.org/10.14407/jrpr.2019.44.1.1.
[22] L. Nenoff, M. Priegnitz, G. Janssens, J. Petzoldt, P. Wohlfahrt, A. Trezza, J. Smeets, G. Pausch, C. Richter, Sensitivity of a prompt-gamma slit-camera to detect range shifts for proton treatment verification, Radiother. Oncol. 125 (2017) 534–540, https://doi.org/10.1016/j.radonc.2017.10.013.